# Feasibility of Cochlea High-frequency Ultrasound and Microcomputed Tomography Registration for Cochlear Computer-assisted Surgery: A Testbed

Mohamed Akkari, Gérard Subsol, Nabil Zemiti, Lucas Lavenir, Charlotte Farah, Florence François, Michel Mondain, Guillaume Captier, Philippe Poignet, Frédéric Venail

# Feasibility of Cochlea High-frequency Ultrasound and Microcomputed Tomography Registration for Cochlear Computer-assisted Surgery: A Testbed

*†Mohamed Akkari, †Gérard Subsol, †Nabil Zemiti, †Lucas Lavenir, ‡Charlotte Farah, §Florence François, *§Michel Mondain, ||Guillaume Captier, †Philippe Poignet, and *§Frédéric Venail

*Department of ENT and Head and Neck Surgery, University Hospital Gui de Chauliac, University of Montpellier; †LIRMM, University of Montpellier, CNRS; ‡IPAM, INSERM U1046, CNRS UMR 9214, University Hospital Arnaud de Villeneuve, University of Montpellier; §Institute for Neurosciences of Montpellier, INSERM U1051, University of Montpellier; and ||Anatomy Laboratory, Medicine Faculty of Montpellier-Nimes, University of Montpellier, Montpellier, France*

**Introduction:** There remains no standard imaging method that allows computer-assisted surgery of the cochlea in real time. However, recent evidence suggests that high-frequency ultrasound (HFUS) could permit real-time visualization of cochlear architecture. Registration with an imaging modality that suffers neither attenuation nor conical deformation could reveal useful anatomical landmarks to surgeons. Our study aimed to address the feasibility of an automated three-dimensional (3D) HFUS/microCT registration, and to evaluate the identification of cochlear structures using 2D/3D HFUS and microCT.

**Methods:** MicroCT, and 2D/3D 40 MHz US in B-mode were performed on ex vivo guinea pig cochlea. An automatic rigid registration algorithm was applied to segmented 3D images. This automatic registration was then compared to a reference method using manual annotated landmarks placed by two senior otologists. Inter- and intrarater reliabilities were evaluated using intraclass correlation coefficient (ICC) and the mean registration error was calculated.

**Results:** 3D HFUS/microCT automatic registration was successful. Excellent levels of concordance were achieved with regards intra-rater reliability for both raters with micro-CT and US images (ICC ranging from 0.98 to 1, $p < 0.001$) and with regards inter-rater reliability (ICC ranging from 0.99 to 1, $p < 0.001$). The mean HFUS/microCT automated RE for both observers was $0.17 \pm 0.03$ mm [0.10–0.25]. Identification of the basilar membrane, modiolus, scala tympani, and scala vestibuli was possible with 2D/3D HFUS and micro-CT.

**Conclusions:** HFUS/microCT image registration is feasible. 2D/3D HFUS and microCT allow the visualization of cochlear structures. Many potential clinical applications are conceivable. **Key Words:** Cochlea—Computer-assisted cochlear surgery—High-frequency ultrasound—Microcomputed tomography—US/CT registration.

Morphological study of the human cochlea is challenging due to its complex anatomy and small size. Current medical imaging techniques have limited spatial resolution that disallows the visualization of cochlear structures, especially the basilar membrane (BM). Indeed, the thickness of the BM varies from 0.2 to 5 μm and its width ranges from 126 μm (base) to 418 μm (apex) (1). The development of computer-assisted surgery (CAS) could greatly improve inner ear surgical procedures, such as cochlear implantation (CI). However, it remains restricted by the spatial resolution of standard imaging modalities (150 μm for cone beam computed tomography [CBCT] (2), 350 μm for 1.5 Tesla MRI (3), 600 μm for classical multidetector computed tomography (4)) and their unsuitability for use in intraoperative imaging.

Brown et al. (5) were the first to publish 2D ultrasound (US) imaging of the human cochlea. Using a 50 MHz array, they were able to visualize the basilar membrane through the round window with 50 μm spatial resolution. This imaging procedure is compatible with real-time in vivo acquisition, and thus could be used as a diagnostic

Address correspondence and reprint requests to Mohamed Akkari, M.D., Department of ENT and Head and Neck Surgery, University Hospital Gui de Chauliac, 80 avenue Augustin Fliche, 34295 Montpellier Cedex 5, France; E-mail: m-akkari@chu-montpellier.fr

This work was supported in part by the French National Agency for Research (Agence Nationale pour la Recherche, ANR) within the Investissements d'Avenir Program (Labex CAMI, ANR-11-LABX0004, the Equipex ROBOTEX, ANR-10-EQPX-44-01).

The authors disclose no conflicts of interest.

tool or integrated into a CAS procedure. Better identification of cochlear architecture could reasonably be envisaged with 3D high-frequency ultrasound (HFUS), yet to our knowledge it has not been reported in the literature. One important obstacle to overcome is attenuation and conical deformation due to US complicating the identification of anatomical structures, especially when measuring through the thick and dense human otic capsule. The use of a lower frequency US of 20 to 40 MHz could provide a better trade-off between resolution and penetration of the US beam into the cochlea. Moreover, registration of perioperative US alongside a preoperative imaging procedure that provides a better anatomical rendering, such as X-ray, could solve the problem of conical deformation. X-ray imaging appears to be more appropriate than MRI for the imaging of cochlear bony structures. Recently, microCT has also shown interesting results for cochlea analysis (6–8), with a spatial resolution ranging from 9 to 36 μm comparable to microscopic histology results (9). The main limitation of microCT is the possibility of processing only small samples, thus narrowing its suitability to small animals and ex vivo human temporal bones.

CT and US bone image registration has already been studied for several anatomical regions (10–13), but not yet for the cochlea. A manual US/CT registration relies on a precise identification of anatomical landmarks in both modalities, and thereby is not only time-consuming but also requires a certain expertise in the field of otology imaging. A reliable automated registration would avoid these two limitations and render the technique more reproducible.

The main objective of this study was therefore to evaluate the feasibility of a 3D automated US/microCT registration that could be used in further works for the development of cochlea CAS. The automated registration modality was to be validated by comparison with a reference manual registration performed by two experts. Our secondary objective was to assess the performance of 2D/3D HFUS and microCT in identifying with sufficient resolution guinea pig cochlear architecture.

## METHODS

Our testbed is presented in Figure 1.

### Cochlea Preparation

All experiments were conducted with the approval of the local ethics committee. We used one ex vivo cochlea removed from a tricolored 350 g female guinea pig, a reference animal model in cochlea studies (14). A lethal intraperitoneal injection of sodium-pentobarbital was performed under general anesthesia. The left temporal bone was removed under a microscope and fixed with paraformaldehyde 4%.

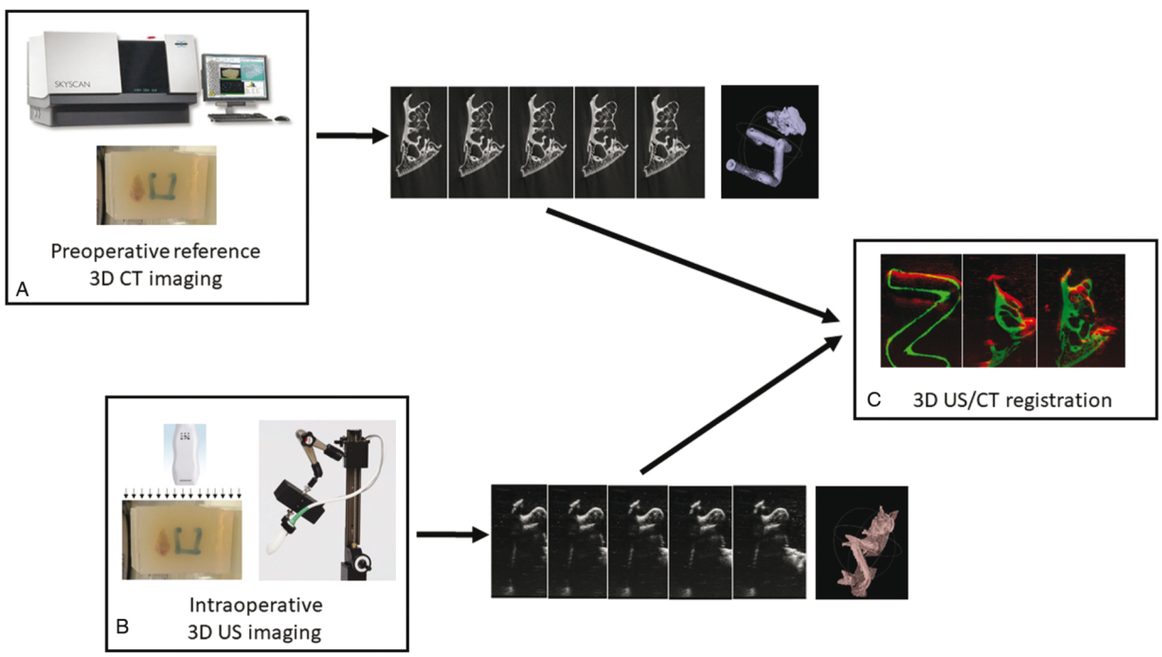


**FIG. 1.** Testbed of our study. We used a bony sample of guinea-pig left cochlea embedded in an agar gel block with a tridimensional fiducial frame to facilitate the registration. *A,* Preoperative reference high-resolution computed tomography (CT) generates a stack of CT slices, with a possibility of multiplanar reconstruction. MicroCT was chosen because it is suitable for small-sized samples and provides higher spatial resolution. *B,* Intraoperative 3D high-frequency ultrasound (US) is performed using a 40 MHz average frequency probe in B-mode coupled with a 3D motor stage. The motor stage and the attached probe travel across the target perpendicular to the imaging orientation, which results in a stack of US slices. Multiplanar reconstruction mode is also available. *C,* The two 3D stacks of images are registered to obtain a fused image, constituting the first step toward the development of a real-time guiding system for computer-assisted surgery of the cochlea.

To facilitate the US/microCT registration, we mounted the cochlea and a tridimensional fiducial frame (FF) in the same block for the 3D US and microCT acquisitions. The FF had to be visible in both US and microCT, and have a specific shape allowing an easy identification and segmentation. It was drafted using the computer-assisted design software Solidworks and manufactured by a rapid prototyping machine (3D printer) Stratasys Fortus 400 mc (Stratasys, Eden Prairie, USA). We chose a triple Z geometric model (1 $cm^3$, 2 mm tube diameter) that had already been validated for stereotactic surgery (15–17). To make it visible in microCT, we covered the FF with a blue layer of commercially available tinted nail polish, in which we added barium sulfate powder (Barium Sulfate ReagentPlus, Sigma-Aldrich, Saint Louis, MO) at 200 g/L (20%) (see supplemental material appendix 1, http://links.lww.com/MAO/B208). To keep a fixed distance between the cochlea and the FF, we embedded both within an agar gel block (50 g/L (5%) in distilled water) (see supplemental material appendix 2, http://links.lww.com/MAO/B209). The gel block was then cut to match the offset and depth characteristics of the US probe.

## MicroCT Acquisitions

To validate the testbed, microCT was chosen over CBCT or classical multidetector computed tomography for its higher spatial resolution and its suitability for small samples.

MicroCT data acquisitions were performed using the technical facilities of the Montpellier Rio Imaging platform and Labex CEMEB. We used the commercialized microCT device Skyscan 1076 (Brucker microCT, Kartuizersweg, Belgium), with X-ray source 20 to 100 kV, spot size $<5$ μm, 10W, X-ray detector 4,000 × 2,672 pixels 12 bit. A multiplanar reconstruction was applied to the native images using the manufacturer's software Nrecon (Brucker microCT), producing an 18 μm isotropic 3D image.

## 2D/3D Ultrasound Acquisitions

The ultrasound device used was the Vevo 2100 Imaging System (Visual Sonics Inc, Toronto, Canada), with a 40 MHz average frequency probe (MS550D, 22–55 MHz operating frequency MicroScan transducer, Visual Sonics Inc.) in B-mode 2D. This probe allows a penetration depth of 15 mm with an offset of 1 mm, and a width of 14.08 mm. Images were taken in several planes to better distinguish the cochlear structures.

To generate a 3D US image, the same device and probe were used in B-mode, coupled with a 3D motor stage. The motor stage and the attached probe travel across the target object in a series of steps, in a direction perpendicular to the imaging orientation. At each step, the transducer acquires one two-dimensional slice. These slices are then combined into a whole image using the manufacturer's software Vevolab (Visual Sonics Inc., Toronto, Canada). Each step (z coordinate) was 0.064 mm apart, with a total distance traveled of 31.75 mm, and number of frames acquired of 500.

## Registration

Bony structures attenuate the US wave, especially at high frequency, as illustrated in Figure 2A, in which the surface of the cochlea is clearly observed while the deeper areas are less well defined. To overcome this limitation, an adapted version of the method described by Brendel et al. (10) was followed. Our strategy was to segment both US and microCT images to strictly work on a common significant part, visible in both modalities, in our case the surface of the cochlea. The 3D images were processed using FIJI (http://fiji.sc/Fiji) open source software.

First, CT and US images were automatically converted into 1-byte images (i.e., with intensity values varying between 0 and 255). A global thresholding was then applied to the 3D microCT based on the value given by Otsu's method (18), which automatically separates background and foreground. The automatic threshold value obtained was 93 (Fig. 2D). For the US image, we manually set the threshold value by visually checking that bony structures were clearly visible while noise was attenuated. The manual threshold value obtained was 150 (Fig. 2B). This process was quick (less than 30 s) and easily achievable as it required neither imaging nor anatomical expertise. It led to binary images where only the white voxels had to be registered.

Second, what part of the microCT image would be visible in the corresponding US dataset was then estimated to generate a ''US simulated'' segmented microCT image. In the US image, where the waves come vertically from the top, the signal was estimated as being attenuated after 0.6 mm. A linear attenuation was thus applied after a column of eight white voxels (corresponding to 0.6 mm) in the microCT image (see Fig. 2E), using our in-house computer application.

The segmented US image was used as the template for registration. An automatic rigid registration algorithm based on the maximization of the standard correlation coefficient between the ''US simulated'' microCT image and the segmented US image was applied. The resulting transformation given by the registration process was then applied to the native microCT image, leading to aligned microCT and US images. A synchronization of the native US image and the aligned unsegmented microCT image visualization windows allowed a first visual appraisal of the registration.

To assess the FF utility, the same procedure was applied to cropped US and microCT images excluding the FF.

## Quantitative Evaluation of the Automated Registration Algorithm Error

The precision of the automatic registration was compared to a manual reference method based on the anatomical skills of two senior otologists experienced in the interpretation of cochlea imaging.

Annotated landmarks were placed by the two otology experts on the 3D native US image. Six points were placed on the cochlea (recognizable landmarks on the surface of the otic capsule or within the cochlea, such as the modiolus for each spiral turn), and six others on the FF (a total of 12 points per expert). The same operation was performed on the aligned unsegmented microCT image (12 points per expert).

Before evaluating the automated registration, the reliability of the manual reference method was first ensured. This was achieved by repeating the landmarks placement procedure five times for every point by each observer (120 points per expert in total) allowing the determination of an intra-rater reliability using intraclass correlation coefficient (ICC, level of significance $p < 0.05$). ICC was calculated separately for cochlear (six points) and FF (six points) annotated landmarks using the five repeated measurements for each observer, with both microCT and US images. Inter-rater reliability was also determined by comparing the average of the five repeated measurements for the cochlea and for the FF between observers using ICC (level of significance $p < 0.05$).

The registration error (RE) between US and microCT images at cochlear and FF annotated landmarks for both observers could then be calculated. The US and microCT coordinates of each point were predicted to be identical in case of a successful alignment. Thus, the distance between the points placed on

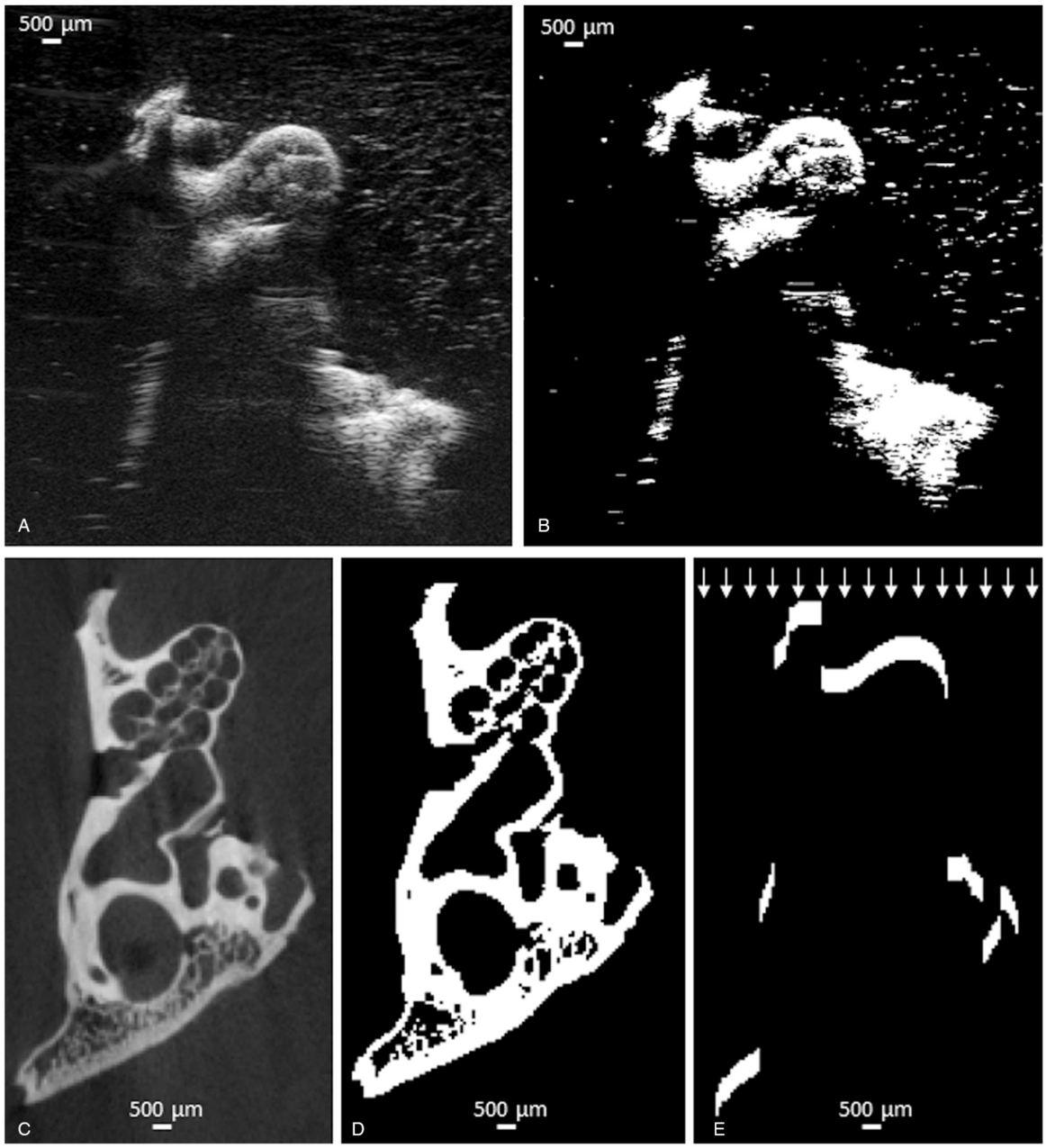


**FIG. 2.** Image preprocessing before registration. *A,* Native US image. *B,* Binary US image after segmentation (thresholding value of 150). *C,* Native microCT image. *D,* Binary microCT image after segmentation (thresholding value of 93). *E,* Binary microCT image after segmentation and "US simulation." White *arrows* show the orthogonal orientation of the "US simulated" waves. Attenuation was applied after 0.6 mm (8 voxels).

microCT and US images was calculated, from which was determined the mean RE (± standard error, [95% confidence interval]) for the cochlea and the FF, either separately for each observer, or as the combination of results from both observers. Finally, the mean RE for cochlea was related to its major axis dimension to determine a relative registration error (RRE).

Calculations and statistics were performed using SPSS 20 software (IBM, Armonk, NY).

## RESULTS

### MicroCT and 2D/3D US Image Generation

Visualization of the BM, modiolus, scala tympani, and scala vestibuli was achieved using both 2D US and microCT. These structures are shown in Figures 3 and 4, at the base and the apex of the cochlea, the height of which was 5 mm.

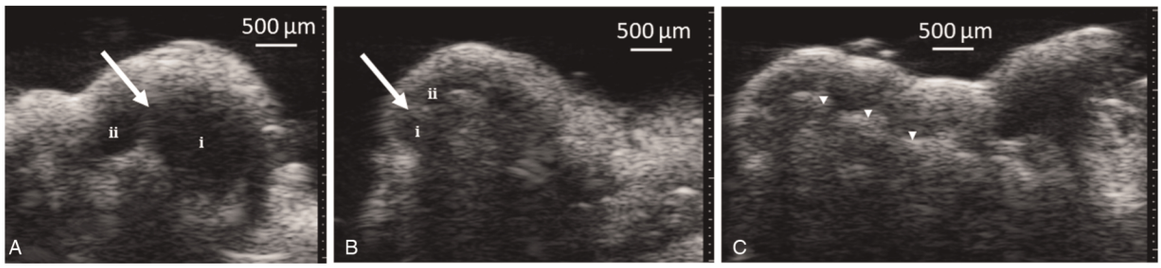


**FIG. 3.** 2D ultrasound of the cochlea. *A,* Visualization of the basilar membrane (BM) (white *arrow*), scala tympani (ST) (i) and scala vestibuli (SV) (ii) at the base of the cochlea. *B*, Visualization of the BM (white *arrow*), ST (i), SV (ii) at the apex of the cochlea. *C,* Longitudinal view of the modiolus all along the cochlea (white *arrowheads*).

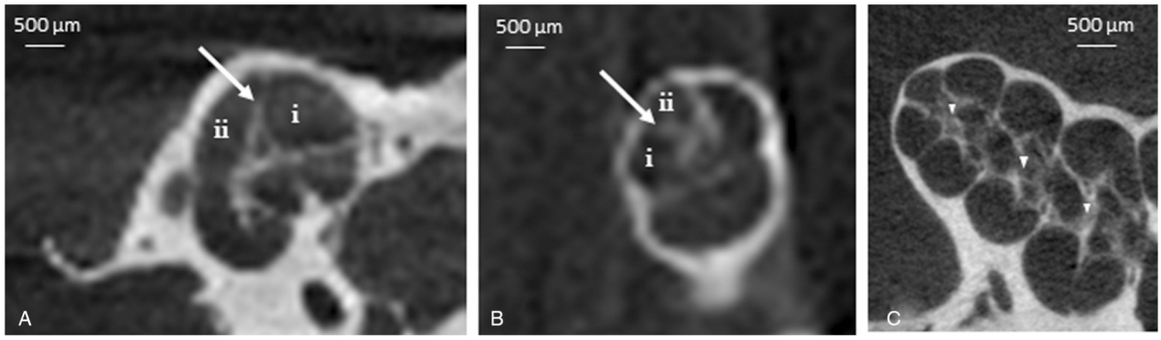


**FIG. 4.** MicroCT of the cochlea. *A,* Visualization of the basilar membrane (white *arrow*), scala tympani (ST) (i) and scala vestibuli (SV) (ii) at the base of the cochlea. *B,* Visualization of the BM (white *arrow*), ST, SV at the apex of the cochlea. *C*, Longitudinal view of the modiolus all along the cochlea (white *arrowheads*).

3D images were successfully generated: 409 slices for US and 1,302 for microCT. Surface reconstructions using FIJI software are shown in Figure 5A and B. Identification of the BM, scala vestibuli, scala tympani, and modiolus was made clearer using the multiplanar reconstruction mode. The image modality providing the best anatomical rendering was microCT, as it was not subjected to the white level generated by noise in US imaging. Furthermore, deeper parts of the bone or the FF had a lower intensity in US than in microCT due to wave attenuation (Fig. 2, A and C).

## Registration

Results of the image processing before registration are shown in Figure 2. The native US image (Fig. 2A) has been simply thresholded (threshold value: 150) (Fig. 2B), while the native microCT image (Fig. 2C) was thresholded (threshold value: 93) (Fig. 2D) before undergoing ''US simulation'' (Fig. 2E).

Once segmented images were aligned, the transformation was applied to the native microCT image. By synchronizing the native US and the aligned unsegmented microCT image windows (duration $< 30$ s), we

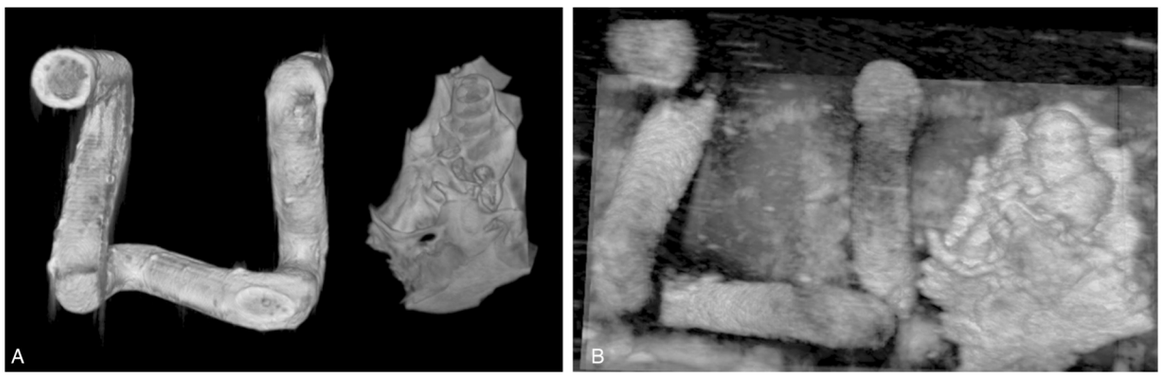


**FIG. 5.** *A,* 3D surface reconstruction of the microCT image. *B,* 3D surface reconstruction of the US image.

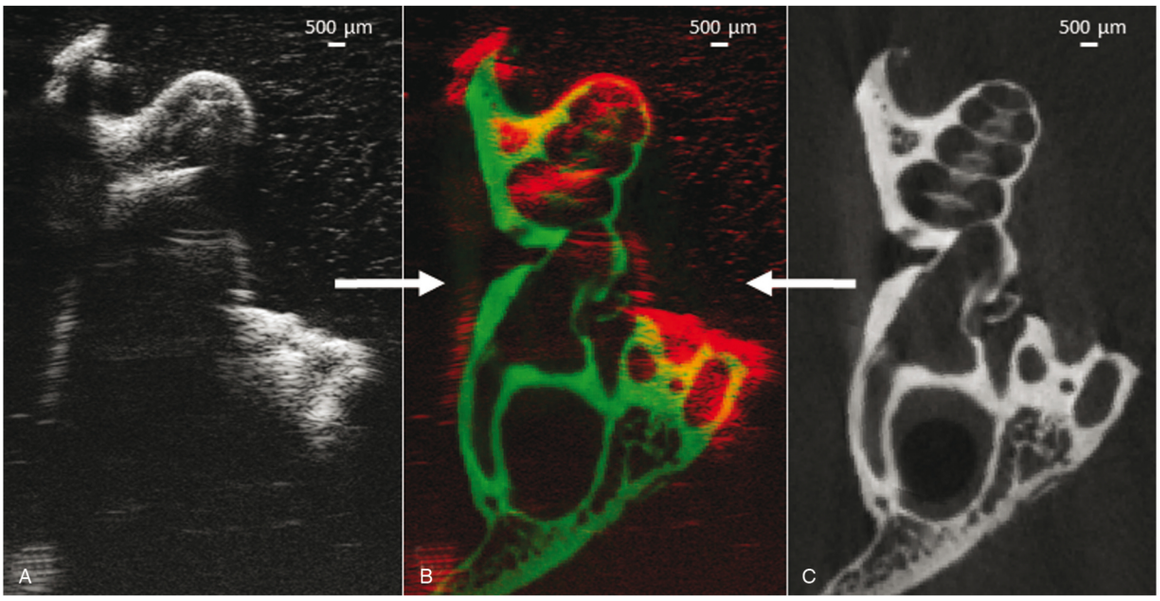


**FIG. 6.** *A,* US native image. *B*, Merged US image (red) and microCT image (green). *C,* microCT image after registration.

were then able to use the combination of both modalities to precisely identify the anatomical structures-of-interest in 3D. By assigning a color to each modality (green for microCT, red for US), we were able to merge them into one image (Fig. 6).

Applying the registration process on cropped images excluding the FF, where only the cochlea was visible, did not allow a successful image alignment.

Calculation of intra-rater reliability showed an excellent concordance among trials for the placement of cochlear annotated landmarks, for both raters, using microCT images or US images (ICC = 1 in both images, $p < 0.001$ for observers 1 and 2). Similar results were found with FF annotated landmarks using microCT (ICC = 0.99, $p < 0.001$ for observers 1 and 2) or US images (ICC = 0.98, $p < 0.001$ for observer 1 and ICC = 1, $p < 0.001$ for observer 2). Inter-rater reliability was also high for cochlear points (ICC = 1, $p < 0.001$ for microCT and US) and for FF points (ICC = 0.99, $p < 0.001$ for microCT and US). These high intra- and inter-rater ICCs confirmed the reliability of manual landmarks placement for use as a reference method.

Mean RE of the automated algorithm for cochlear points compared with manual registration was $0.23 \pm 0.04$ mm [0.14–0.32] for observer 1, $0.17 \pm 0.03$ mm [0.11–0.24] for observer 2, and $0.17 \pm 0.03$ mm [0.10–0.25] for both observers combined. This value was related to the cochlea height of 5 mm, leading to a RRE of 0.034 (see supplemental material appendix 3, http://links.lww.com/MAO/B210).

Registration errors were higher for FF points with a mean RE of $0.38 \pm 0.07$ mm [0.23–0.53] for observer 1, $0.39 \pm 0.08$ mm [0.23–0.56] for observer 2, and $0.38 \pm 0.07$ mm [0.22–0.54] for both observers combined.

## DISCUSSION

Being able to visualize and preserve the BM might help to detect and overcome difficult surgical situations during CI, such an altered anatomy or intrascalar fibrosis. In addition, preservation of cochlear architecture during CI is necessary to maintain the residual insufficient but still useful hearing intact. Indeed, insertion of the electrode array is associated with frictional forces (19) that cause anatomical damage and compromise the preservation of remaining hearing (20,21). Imaging guidance may also prove useful in specific and safe drug delivery to the inner ear. While infusion-based inner ear drug delivery methods have been assessed in animal models (22), they have not been transposed to patients so far because of the potential harmful effects on hearing. Indeed, although the scala tympani insertion may not need imaging guidance, the direction of the inserted catheter or device cannot be monitored and may cause scala translocation, as shown in CI.

The potentially easy and cost-effective implementation of HFUS during surgery to ensure damage-free visualization of the inner ear ultrastructure (23) makes it a promising imaging modality for the improvement of CI techniques. Intraoperative visibility of CI electrodes, using US imaging (24), could help detect a misplaced device, thus avoiding reoperation. Landry et al. have demonstrated the feasibility of combining HFUS, automated CI insertion, and force sensing to monitor CI insertion dynamics in decalcified cadaver cochlea (24). These results are not applicable in vivo due to the need for cochlea decalcification. Previous studies carried out without decalcification showed that the visualization of the cochlea with a 50 MHz probe was limited to a depth

of 5 mm, which is not sufficient to conduct an intracochlear procedure.

US-CT registration has been reported to be a complex procedure (10,12,13,25–28). According to one review of the literature by Hacihaliloglu et al. (12), described methods can be classed into two categories: surface-based and intensity-based registration. Either way, most described methods concerned less complex and significantly larger bone structures compared with cochlea (25,28,29). With regards the surface-based approaches, two main difficulties encountered were achieving an accurate segmentation of bone surfaces in US data, and an accurate initial alignment between the two modalities to guide the registration. We therefore decided to use an intensity-based method for which we chose the correlation criterion as the most suitable among the several matching criteria assessed in the literature (10,11,29,30). The use of binary thresholded images (11) allows us to work on images less affected by noise. The threshold values we defined using FIJI software are applicable to future samples. Simulation of US images from CT, such as we performed, has been described in the literature (10,31). However, the thresholding method and the attenuation simulation that we employed remain rudimentary and warrant refining. For instance, a sensitivity analysis of the RE as a function of different levels of thresholding could be interesting in future works.

At first glance, the mean automated algorithm RE of 0.17 mm seems better than the 0.5 mm previously reported by Brendel et al. in their study on the spine (10), or the 1.6 mm reported by Penney et al. in their study on the pelvis (13,28). However, the distance error must be interpreted with regards to the dimensions of the studied organ, which is not so easy considering the anatomic complexity of each organ. As a rough comparison, our RRE was 0.034, versus 0.0625 for Brendel et al. (relating to an 8 cm major axis of the vertebra) and 0.08 for Penney et al. (relating to a 20 cm major axis of the hip bone).

The difference between the mean distance errors based either on the cochlea landmarks or on the FF landmarks is remarkable, leading to question of the choice of FF geometry. Indeed, a parallelepiped shape might have been more appropriate for land-marking than the cylindrical frame we used. The registration failure observed in the present feasibility study when only considering the cochlea would support the relevance of using a FF. However, the registration algorithm needs refining in future in vivo works toward one that no longer requires the FF. One way of doing this may be modifying the segmentation to reduce the noise from the US image and increase the number of black and white voxels, thereby obtaining a better alignment using the standard correlation criterion. Another possibility would be to depend on a ''natural'' FF such as the ossicular chain that displays very specific geometry that is clearly visible with US (32).

Our study presents promising results for the morphological study of the cochlea using 2D and 3D US. Wave attenuation and noise remain the two main limitations. The main cause of attenuation in our setup was the interposition of thick bone. The challenge would be even greater if applied to human temporal bone known to be denser than that of the guinea pig. This problem was experimentally overcome by other teams using previous bone thinning or decalcification (24), yet obviously remains unavoidable with in vivo procedures. Considering that the higher the frequency of US, the higher the spatial resolution and the shallower the depth of penetration, one could choose to favor increased depth at the expense of resolution. Nevertheless, this limitation justifies all the more the need for registration with a CT-based imaging to compensate for the lack of anatomical rendering.

A next step toward in vivo application of our approach will be the use of CBCT instead of microCT, raising the issue of its insufficient spatial resolution to visualize cochlear structures. Nevertheless, Zou et al. have validated the reliability of CBCT compared with microCT in identifying the scalar location of cochlear implant electrode after round window insertion (33). Other publications have confirmed that while CBCT is unable to actually visualize the BM, it is reliable to assess an electrode array placement in the scala tympani in human temporal bones (34,35). Consequently, it could be used in future works for US/CT registration to compensate for the US limitations described above.

We used a commercially available high-frequency device, which does not have suitable dimensions for in vivo procedures. The latter would require a relevant placement of the US probe, which is achievable if using a miniaturized probe able to be inserted through the eardrum to fit the middle ear dimensions. Significant advances have been made to this end (36), especially by Brown's team who designed a miniaturized high-frequency endoscopic phased array (37,38). Another limitation of our study is that all experiments were carried out on one cochlea; more datasets would indeed have helped improve statistical power. Nevertheless, we consider our experimental setup as a representable one that led to reliable results, especially the feasibility of a US/microCT registration. Finally, even if not assessed in our study, it is noteworthy that US can be used to perform vibrometry, a useful feature to study intracochlear dynamics (4,23,38,39).

## CONCLUSIONS

Our study confirms that US/microCT automated registration is feasible using a rigid registration algorithm based on the standard correlation criterion, and thus has many potential clinical applications. In addition, 2D/3D HFUS allows the visualization of small structures in the vicinity of the cochlea, especially the BM. Together, the 3D HFUS and microCT offer the possibility of multiplanar reconstruction and image processing that provide a clearer visualization.

Our future works will focus on improving this innovative approach by attempting to overcome several challenges: 1) coming up with an FF-independent

algorithm; 2) determining the optimum US frequency offering the right balance between spatial resolution and wave attenuation in human cadaver ex situ temporal bone; 3) assessing the use of CBCT instead of microCT for US/CT registration; 4) designing a miniaturized US probe for safe in vivo applications.

**Acknowledgments:** The authors thank the Groupe d'Etude des Maladies de l' Oreille (GEMO) that funded Dr Mohamed Akkari's Master 2 thesis internship during which this study was performed.

The authors also thank Dr Renaud Lebrun (Montpellier Rio Imaging platform and LabEx CeMEB – Institut des Sciences de l'Evolution – Université de Montpellier – CNRS UMR 5554 – Campus Triolet Place Eugène Bataillon 34095 Montpellier Cedex 5) for contribution in the microCT image acquisition.

## REFERENCES

1. Liu W, Atturo F, Aldaya R, et al. Macromolecular organization and fine structure of the human basilar membrane—RELEVANCE for cochlear implantation. *Cell Tissue Res* 2015;360:245–62.
2. Miracle AC, Mukherji SK. Conebeam CT of the head and neck, part 2: Clinical applications. *AJNR Am J Neuroradiol* 2009;30: 1285–92.
3. Wiet GJ, Schmalbrock P, Powell K, Stredney D. Use of ultra-high-resolution data for temporal bone dissection simulation. *Otolaryngol Head Neck Surg* 2005;133:911–5.
4. Bance M, Zarowski A, Adamson RA, Casselman JW. New imaging modalities in otology. *Adv Otorhinolaryngol* 2018;81:1–13.
5. Brown JA, Torbatian Z, Adamson RB, et al. High-frequency ex vivo ultrasound imaging of the auditory system. *Ultrasound Med Biol* 2009;35:1899–907.
6. Braun K, Bohnke F, Stark T. Three-dimensional representation of the human cochlea using micro-computed tomography data: Presenting an anatomical model for further numerical calculations. *Acta Otolaryngol* 2012;132:603–13.
7. Shin KJ, Lee JY, Kim JN, et al. Quantitative analysis of the cochlea using three-dimensional reconstruction based on microcomputed tomographic images. *Anat Rec (Hoboken)* 2013;296:1083–8.
8. Sun CC, Jiang ZD, Zhang K. Micro-CT imaging of guinea pig cochlear. *Zhonghua Yi Xue Za Zhi* 2012;92:3442–4.
9. Buytaert JA, Johnson SB, Dierick M, Salih WH, Santi PA. MicroCT versus sTSLIM 3D imaging of the mouse cochlea. *J Histochem Cytochem* 2013;61:382–95.
10. Brendel B, Winter S, Rick A, Stockheim M, Ermert H. Registration of 3D CT and ultrasound datasets of the spine using bone structures. *Comput Aided Surg* 2002;7:146–55.
11. Brounstein A, Hacihaliloglu I, Guy P, Hodgson A, Abugharbieh R. Towards real-time 3D US to CT bone image registration using phase and curvature feature based GMM matching. *Med Image Comput Comput Assist Interv* 2011;14 (pt 1):235–42.
12. Hacihaliloglu I, Wilson DR, Gilbart M, Hunt MA, Abolmaesumi P. Non-iterative partial view 3D ultrasound to CT registration in ultrasound-guided computer-assisted orthopedic surgery. *Int J Comput Assist Radiol Surg* 2013;8:157–68.
13. Penney GP, Barratt DC, Chan CS, et al. Cadaver validation of intensity-based ultrasound to CT registration. *Med Image Anal* 2006;10:385–95.
14. Katsumi S, Sahin MI, Lewis RM, Iyer JS, Landegger LD, Stankovic KM. Intracochlear perfusion of tumor necrosis factor-alpha induces sensorineural hearing loss and synaptic degeneration in guinea pigs. *Front Neurol* 2019;10:1353.
15. Masamune K, Fichtinger G, Patriciu A, et al. System for robotically assisted percutaneous procedures with computed tomography guidance. *Comput Aided Surg* 2001;6:370–83.
16. Lee S, Fichtinger G, Chirikjian GS. Numerical algorithms for spatial registration of line fiducials from cross-sectional images. *Med Phys* 2002;29:1881–91.
17. DiMaio SP, Samset E, Fischer G, et al. Dynamic MRI scan plane control for passive tracking of instruments and devices. *Med Image Comput Comput Assist Interv* 2007;10 (Pt 2):50–8.
18. Otsu N. A threshold selection method from gray-level histograms. *IEEE Trans Syst Man Cybern* 1979;9:62–6.
19. Nguyen Y, Kazmitcheff G, De Seta D, Miroir M, Ferrary E, Sterkers O. Definition of metrics to evaluate cochlear array insertion forces performed with forceps, insertion tool, or motorized tool in temporal bone specimens. *Biomed Res Int* 2014;2014:532570.
20. Miranda PC, Sampaio AL, Lopes RA, Ramos Venosa A, de Oliveira CA. Hearing preservation in cochlear implant surgery. *Int J Otolaryngol* 2014;2014:468515.
21. Snels C, IntHout J, Mylanus E, Huinck W, Dhooge I. Hearing preservation in cochlear implant surgery: A meta-analysis. *Otol Neurotol* 2019;40:145–53.
22. Ibrahim HN, Bossard D, Jolly C, Truy E. Radiologic study of a disposable drug delivery intracochlear catheter. *Otol Neurotol* 2011;32:217–22.
23. Landry TG, Bance ML, Adamson RB, Brown JA. No effect of prolonged pulsed high frequency ultrasound imaging of the basilar membrane on cochlear function or hair cell survival found in an initial study. *Hear Res* 2018;363:28–38.
24. Landry TG, Earle G, Brown JA, Bance ML. Real-time intracochlear imaging of automated cochlear implant insertions in whole decalcified cadaver cochleas using ultrasound. *Cochlear Implants Int* 2018;19:255–67.
25. Wein W, Karamalis A, Baumgartner A, Navab N. Automatic bone detection and soft tissue aware ultrasound-CT registration for computer-aided orthopedic surgery. *Int J Comput Assist Radiol Surg* 2015;10:971–9.
26. Klauser AS, De Zordo T, Feuchtner GM, et al. Fusion of real-time US with CT images to guide sacroiliac joint injection in vitro and in vivo. *Radiology* 2010;256:547–53.
27. Caskey CF, Hlawitschka M, Qin S, et al. An open environment CT-US fusion for tissue segmentation during interventional guidance. *PLoS One* 2011;6:e27372.
28. Barratt DC, Penney G, Chan CS, et al. Self-calibrating ultrasound-to-CT bone registration. *Med Image Comput Comput Assist Interv* 2005;8 (pt 1):605–12.
29. Firle E, Wesarg S, Dold C. Mutual-information-based registration for ultrasound and CT datasets. Proc. SPIE 5370, Medical Imaging 2004: Image Processing, 1130 (May 12, 2004); doi:10. 1117/12. 534572. *Med Imaging* 2004;2004:1130–8.
30. Roche A, Pennec X, Malandain G, Ayache N. Rigid registration of 3-D ultrasound with MR images: A new approach combining intensity and gradient information. *IEEE Trans Med Imaging* 2001;20:1038–49.
31. Wein W, Brunke S, Khamene A, Callstrom MR, Navab N. Automatic CT-ultrasound registration for diagnostic imaging and image-guided intervention. *Med Image Anal* 2008;12:577–85.
32. Rainsbury JW, Landry TG, Brown JA, Adamson RA, Bance M. High frequency ex vivo ultrasound imaging of the middle ear to show simulated ossicular pathology. *Otol Neurotol* 2016; 37:586–92.
33. Zou J, Hannula M, Lehto K, et al. X-ray microtomographic confirmation of the reliability of CBCT in identifying the scalar location of cochlear implant electrode after round window insertion. *Hear Res* 2015;326:59–65.
34. Dietz A, Gazibegovic D, Tervaniemi J, Vartiainen VM, Lopponen H. Insertion characteristics and placement of the Mid-Scala electrode array in human temporal bones using detailed cone beam computed tomography. *Eur Arch Otorhinolaryngol* 2016; 273:4135–43.
35. Zou J, Lahelma J, Koivisto J, et al. Imaging cochlear implantation with round window insertion in human temporal bones and cochlear morphological variation using high-resolution cone beam CT. *Acta Otolaryngol* 2015;135:466–72.

36. Khuri-Yakub BT, Oralkan O, Nikoozadeh A, et al. Miniaturized ultrasound imaging probes enabled by CMUT arrays with integrated frontend electronic circuits. *Conf Proc IEEE Eng Med Biol Soc* 2010;2010:5987–90.
37. Bezanson A, Adamson R, Brown J. Fabrication and performance of a miniaturized 64-element high-frequency endoscopic phased array. *IEEE Trans Ultrason Ferroelectr Freq Control* 2014;61:33–43.
38. Torbatian Z, Garland P, Adamson R, Savage J, Bance M, Brown J. Listening to the cochlea with high-frequency ultrasound. *Ultrasound Med Biol* 2012;38:2208–17.
39. Landry TG, Bance ML, Leadbetter J, Adamson RB, Brown JA. In vivo measurement of basilar membrane vibration in the unopened chinchilla cochlea using high frequency ultrasound. *J Acoust Soc Am* 2017;141:4610.